Anticipating the occurrence and type of critical transitions

Florian Grziwotz
Westfalian Wilhelms-Univerity Münster
Chen-Wei Chang
National Center for Theoretical Sciences https://orcid.org/0000-0002-9817-2956
Vasilis Dakos
Université de Montpellier https://orcid.org/0000-0001-8862-718X
Egbert Van Nes
Wageningen University
Markus Schwarzländer
Westfalian Wilhelms-Univerity Münster https://orcid.org/0000-0003-0796-8308
Oliver Kamps
Westfalian Wilhelms-University Münster
Martin Hessler
Westfalian Wilhelms-University Münster https://orcid.org/0000-0003-0529-7926
Isao Tokuda
Ritsumeikan University https://orcid.org/0000-0001-6212-0022
Arndt Telschow
Westfalian Wilhelms-University Münster
Chih-hao Hsieh (chsieh@ntu.edu.tw)
National Taiwan University https://orcid.org/0000-0001-5935-7272

Article

Keywords:

Posted Date: April 6th, 2022

DOI: https://doi.org/10.21203/rs.3.rs-1397318/v1

Prepared for Letters in Nature Sustainability

Date of preparation: 2022/02/25

Anticipating the occurrence and type of critical transitions

Florian Grziwotz[1+], Chun-Wei Chang[2+], Vasilis Dakos[3], Egbert H. van Nes[4], Markus Schwarzländer[5], Oliver Kamps[6], Martin Hess[6], Isao T. Tokuda[7], Arndt Telschow[1,8*], Chih-hao Hsieh[2,9,10,11*]

Affiliations:

[1]Institute for Evolution and Biodiversity, Westphalian Wilhelms-University Münster, Münster, 48149 Germany

[2]National Center for Theoretical Sciences, Taipei 10617, Taiwan

[3]ISEM, University of Montpellier, CNRS, EPHE, IRD, Montpellier, France

[4]Aquatic Ecology and Water Quality Management Group, Wageningen University, Wageningen, The Netherlands

[5]Institute of Plant Biology and Biotechnology, University of Münster, 48143 Münster, Germany

[6]Center for Nonlinear Science, Universität of Münster, Münster, Germany

[7]Department of mechanical engineering, Ritsumeikan University, Kusatsu 525-8577, Japan

[8]Institute for Environmental Systems Science, University of Osnabrück, Osnabrück, 49076 Germany

[9]Research Center for Environmental Changes, Academia Sinica, Taipei 11529, Taiwan

[10]Institute of Oceanography, National Taiwan University, Taipei 10617, Taiwan

[11]Institute of Ecology and Evolutionary Biology, Department of Life Science, National Taiwan University, Taipei 10617, Taiwan

[+]Equal contribution

*Correspondence to: Arndt Telschow (telschow@uni-muenster.de) and Chih-hao Hsieh (chsieh@ntu.edu.tw)

Abstract

A critical transition can occur in many real-world systems and the ability to forecast the occurrence of transition is of major interest in a range of contexts. Various early warning signals (EWS) have been developed to anticipate a critical transition or distinguish types of transitions. However, there is no effective method to establish practical thresholds indicating the condition when a critical transition is most likely to occur. Here, we introduce a powerful EWS, named Dynamical Eigen-Value (DEV), rooted in bifurcation theory of dynamical systems, that estimates the dominant eigen-value of the system. Theoretically, the absolute value of DEV approaches 1 when the system approaches bifurcation, whereas its position in the complex plane indicates the type of transition. We demonstrate the efficacy of the DEV approach in model systems with known bifurcation types and in addition we test the DEV approach on various critical transitions in real-world systems.

Introduction

There is a growing consensus that many real-world systems have a critical threshold (i.e., tipping point)[1-5], at which systems suddenly shift to a distinct state, i.e., critical transitions initiated by local bifurcation[6], e.g., outbreak of desert locusts[7], development of psychiatric disorders[2], or rapid global warming at the end of glacial periods[8]. Critical transitions may shift a system to a new state with undesirable properties, causing damage and loss in environmental, economic, and public health resources in the absence of timely corrective action. Thus, it is important for various fields and in many applications to forecast occurrence and consequence of critical transitions.

Many early warning signals (EWS) have been proposed to anticipate upcoming critical transitions[9]. However, most EWS can only warn of a critical transition in a qualitative way or do not perform consistently for different types of critical transition. According to bifurcation theory, when the system is approaching a tipping point, the system starts to recover more slowly from local perturbations[10-12], as the dominant eigenvalue goes to 0 in continuous systems or to 1 in discrete systems. This so-called critical slowing down (CSD)[9] can be revealed by increases in generic EWS[10], including increasing autocorrelation (e.g., AR1[5]) and variability (e.g., SD[13]) in time series. It was suggested that AR1 and SD will reach 1 and infinity, respectively at the tipping point, if dynamical systems can be locally approximated by a first-order stochastic process[5,9]. However, these thresholds were usually not met in real-world critical transitions[5] or even in model systems[14,15]. For example, AR1 does not reach 1 for Neimark-Sacker bifurcation (Fig. S1). Existing EWS are developed for anticipating critical transitions in fold bifurcation[16] (i.e., catastrophe shift[1]) but may not distinguish fold bifurcation from more complex types of bifurcations[16,17] (e.g., Hopf or Neimark-Sacker bifurcation).

Recognizing that various types of bifurcation bring divergent consequences to our focal systems that need different corresponding management to minimize potential losses, a recent study using deep-learning had promise to distinguish types of bifurcation[17]; however, this approach cannot predict the upcoming critical transition and is not rooted in the theory of dynamical system. Moreover, the method based on deep-learning strongly depends on the training set and is so far difficult to apply in high-dimensional cases. Practically, there is no method providing a precise threshold for indicating how large the

raised EWS shall be, beyond which critical transition is deemed to occur, and also indicating the type of transition.

The solution for the challenge is hinted in bifurcation theory - the types and conditions for the occurrence of critical transition are quantitatively determined based on the dominant eigen-value derived from locally linearized dynamical systems[6,18] (i.e., Jacobian matrices; Box 1). When the critical transition occurs at the tipping point, the absolute value of the dominant eigen-value increases to 1 (in discrete systems)[19]. Moreover, various bifurcation types are distinguishable by examining the dominant eigen-value on a complex plane[19]. Despite these well-established theoretical arguments, a critical challenge in their implementation remains that such a dominant eigen-value can only be derived if all parametric equations governing dynamical systems can be determined. However, the equations (or even their parameters) are generally unknown (or difficult to estimate) in real-world systems. Recent advances in time series analysis of dynamical systems indicate that Jacobian (interaction) matrix as well as its dominant eigen-value can be estimated by the recently advanced lag-embedding empirical dynamical modeling (EDM)[20,21] requiring no model assumptions. However, the existing method of computing dominant eigen-value (known as local Lyapunov stability)[24] requires full information of all interacting components (e.g., interacting species) that is usually not readily available, especially in large systems. Therefore, the existing method used to quantify dominant eigen-value[24] might not be a suitable EWS and cannot be easily applied in most systems.

We propose Dynamical Eigen-Value (DEV) as a novel EWS derived from EDM[20,25] that analyzes time series data requiring no specific model assumption[22] (e.g., no need to assume time-varying autocorrelated stochastic process[23]). The proposed DEV directly estimates the dominant eigen-value of focal systems instead of indirectly quantifying phenomena accompanying critical slowing down, as previous EWS. Therefore, as suggested in bifurcation theory, this novel EWS has a quantitative threshold for the occurrence of critical transition (the absolute value of the estimated dominant eigen-value |DEV|=1) and can differentiate types of critical transition by examining DEV on a complex plane (Box 1 presents critical transitions induced by fold, period-doubling, and Neimark-Sacker bifurcations). The presence of DEV threshold enables us to not only

present a qualitative increasing/decreasing trend of EWS in a relative sense (like most existing EWS), but explicitly quantify system resilience in an absolute sense. That is, the absolute value of DEV itself is meaningful and can be directly compared to a theoretical threshold rather than just compared to values estimated in previous time windows. Unlike the existing EDM method in computing dominant eigen-value[24], DEV recovers the whole system dynamics from a single time series using lag embeddings[26] (i.e., Takens theorem[27]), requiring no full information of interacting components. Implementation of DEV also relaxes the assumption underlying general EDM methods[24,28] that critical properties of the system (e.g., model parameters) are constant throughout the sampling period. This assumption unlikely holds in critical transition, during which at least one bifurcation parameter changes with time[14]. Therefore, the proposed DEV enables tracking temporal changes in system resilience (see details in Methods) and is rooted in bifurcation theory that quantitatively reveals both the occurrence condition and type of critical transition[19].

To validate the efficacy of DEV approach, we used three model time series datasets demonstrating known fold, period-doubling, and Neimark-Sacker bifurcations. Then, we empirically tested the DEV method in real-world cases of critical transitions from cell-level experiments to global scale paleoclimatic events (Tables S1 and S2). For each dataset, we computed DEV that anticipated the occurrence and type of critical transition in both model and empirical cases, following procedures summarized in Fig. S2.

Results

Validation of DEV using model data

We examined three discrete-time nonlinear dynamical models (Table S1), Noy-Meir model, Hénon map, and Rosenzweig-MacArthur model (Fig. 1a, b), representing fold, period-doubling, and Neimark-Sacker bifurcation, respectively. The derived DEV reliably estimated the dominant eigen-values of nonlinear dynamical systems and mimicked its dynamical behavior when approaching bifurcation. Specifically, the |DEV| monotonically increased when approaching the tipping point and reached 1 when the system was at the tipping point (Fig. 1c). Moreover, mapping DEV to the complex plane clearly distinguished various types of bifurcation (Fig. 1d), where Re(DEV)→1 and Im(DEV)→

0 for fold bifurcation; Re(DEV)→−1 and Im(DEV)→0 for period-doubling bifurcation; Im(DEV)≠0 and |DEV| → 1 for Neimark-Sacker bifurcation. Consequently, the estimated DEV as a reliable EWS anticipated the occurrence of critical transition (i.e., tipping point) (Fig. 1c), regardless of bifurcation type. Results obtained from discrete-time models were similar to their continuous-time analogues (Fig. S3). Therefore, DEV was an effective EWS that anticipated critical transition with a certain threshold (|DEV|=1) and correctly distinguished various types of bifurcation in model systems.

Next, we evaluated efficacy of DEV when including noise (e.g., observation error and process noise). In the presence of noise, DEV remained a proper EWS (Fig. S4-6) that monotonically increased when approaching the tipping points, but the quantitative threshold of |DEV| was not necessarily equal to 1 at the tipping point. Nevertheless, under small to moderate levels of noises, DEV still correctly identified types of bifurcation (Fig. S7). Through this sensitivity analysis, the estimated DEV in model systems remained effective with noise, except the Rosenzweig-MacArthur model (which is more sensitive to observation noise; Fig. S6). Perhaps the Rosenzweig-MacArthur model showing Neimark-Sacker bifurcation has more complicated mathematical *normal form*[29] with higher order terms likely amplifying impacts of noises. Nonetheless, under reasonable degrees of noise, our DEV method determined that Neimark-Sacker bifurcation occurred in real-world cases (e.g., Fig. 2d-f).

DEV analysis of empirical time series

We investigated five empirical examples, including a cyanobacteria microcosm experiment under light stress, a physical experiment of voice production during phonation onset, cytosolic ATP dynamics in living plant tissues under progressive hypoxia, calcium carbonate ($CaCO_3$) abundance by the end of greenhouse Earth, and bus voltage frequency before power grid failure (Table S1-2), and anticipated the occurrence and type of critical transition (Fig. 2). For empirical systems, |DEV| increased when approaching the tipping point and almost reached 1 at the tipping point (Fig. 2 b, e, h, k, n). Therefore, we inferred the theoretical threshold (|DEV|=1) was still meaningful in empirical systems, despite noise in empirical data. In addition, the computed DEV clearly differentiated types of critical transition in empirical cases (Fig. 2c, f, i, l, o). Among

these examples, only the voice experiment had Neimark-Sacker bifurcation (with a nonzero imaginary part), whereas all others demonstrated fold bifurcation. This conclusion was robust against various choices of embedding parameters (e.g., E, τ, and window size) (Fig. S8-S12). Identification of bifurcation type provided important insights into foreseeing the coming new state of the system. Clearly, fold-type critical transition shifts systems to a new regime with a distinct state (e.g., Fig. 2j), whereas Neimark-Sacker bifurcation shifts systems to a new regime with higher temporal variability (e.g., Fig. 2d). Information regarding bifurcation type enables more appropriate management strategies to cope with new regimes.

Reliability tests of DEV method

Whereas DEV is a quantitative EWS with a theoretical threshold, its efficacy is likely undermined by observation and process noises (e.g., |DEV|<1 and more gradual increase of |DEV| approaching bifurcation; Fig. S4-6). Underestimation of DEV under strong noises was attributed to the dominant eigen-value of pure stochastic processes being 0, leading to synthesized signals with DEV < 1 at the tipping point. Therefore, caution is needed when considering the derived DEV, especially at the tipping point. Here, we suggest that the uncertainty of DEV can be evaluated by its predictability on future states (e.g., the correlation coefficient (ρ) between observed and predicted one-step forward future states; Fig. 3) because predictability is an effective indicator for evaluating the uncertainty of reconstructed dynamical systems[30]. Indeed, there was a high association between the predictability and the uncertainty of estimated DEV defined as how far the estimated DEV is to the analytically solved dominant eigen-value (without noise). When predictability was high, the |DEV| reached almost 1 prior to transition, whereas the |DEV| did not reach 1 (Fig. S4-6) when predictability was low under strong noises (Fig. 3). Thus, system predictability provided indications for precautionary decisions regarding the threshold.

Discussion

Implications from analyzing empirical data

Based on analyses of empirical data, the DEV method can be applied to various

fields (Fig. 2). This is remarkable not only because of diverse underlying systems, but also due to huge differences in temporal and spatial scales that range from milli-seconds and micro-meters in cellular processes to millions of years and thousands of kilometers in climate dynamics. Nonetheless, there is one common feature: the underlying dynamics are governed by feedback mechanisms, a typical characteristic of nonlinear dynamical systems. Such feedback regulations might lose controls due to external forcing; consequently, a critical transition occurs[18]. Therefore, an analytical framework that acknowledges feedbacks and nonlinearity, e.g., our DEV method rooted in nonlinear time series analysis[20], has wide applicability for anticipating occurrence of critical transition under various spatiotemporal scales.

Existing methods for anticipating a critical transition are *qualitative* in the sense that statements can be made only about whether a system is moving towards a tipping point or not. In comparison, the most novel aspect of the DEV method is that a *quantitative* statement can be made regarding the extent that current DEV values from the theoretical threshold (i.e., |DEV|=1) present a sufficient and necessary condition of mathematical bifurcation[19] (i.e., critical transition). In addition to being an EWS, this quantitative feature enables assessment of system resilience even if the analysis was only done within one time window with a few portions of time series data. For example, the |DEV| values estimated from the last time windows before critical transition (300 data points), were 0.99, 0.99, 1.01, 0.91, 0.99 for microcosm, voice, cellular energy, climate, and power grid data, respectively, indicating that all examined system states were at or close to a tipping point. Therefore, DEV correctly anticipated the ongoing critical transition without relying on measures estimated in previous time windows (i.e., a need to uncover a trend of declining system resilience in a relative sense). Although great care must be taken with estimates, we concluded that the DEV method is a major advance in improving the accuracy of the resilience and risk assessment of a wide variety of empirical systems.

Applying DEV analysis to the microcosm experiment was a novel way to quantitatively forecast catastrophic consequences of biological populations. A central issue in population biology is to predict fates of populations (e.g., preservation or extinction of species or species invasion) when facing various stressors. Although predictions can be made from numerous models, implementation of most population

models requires correct identification of both model structure and parameters[31], which seldomly match in empirical cases. In contrast, our DEV analysis characterizes population dynamics without detailed information about model structure and parameter. Nonetheless, unlike most model-free EWS[32], DEV as an empirical estimate of dominant eigen-value allows to be analyzed as that in theoretical population models (e.g., bifurcation analysis). Therefore, the proposed DEV links model-free EWS to analysis of parametric models, with excellent research potential.

Exceptionally good results were achieved for cellular energy status and voice production (Fig. 2d-i), implying cell biology and physiology have promise for future DEV applications. Both research fields have been rarely mentioned in previous EWS literature, although many types of time series data with high spatiotemporal resolution can be generated using modern imaging and -omics techniques. Therefore, DEV may have broad applications, including investigating various cellular and physiological switches that are critical to organism functions. These switches often lead to diseases (e.g., cancer), whereas dysfunction in energy transformation within mitochondria is linked to aging[33] or disease[34]. Our proposed DEV may serve as a warning signal early in disease development, facilitating early treatment.

Critical transition has important roles in driving climate events at global scale (Fig. 2j-l). Our findings confirmed that a critical transition occurred by the end of last greenhouse earth[5]. Our proposed method further characterized this global-scale shift as fold bifurcation. In this case, mean air temperature abruptly declined and then terminated greenhouse earth. Compared to analyses of other empirical cases (Fig. 2b, e, h, n), the DEV measures derived from paleoclimate data, although significantly increased, had noticeable underestimation around the tipping point (i.e., < 1 in Fig. 2k). Such underestimation was likely caused by noises introduced when inferring ancient climate conditions from geological climate proxy or by lacking spatial information (i.e., time series from a single site) in analyzing inherently spatial global-scale climate dynamics.

Our analysis of voltage frequency data preceding a power grid failure (Fig. 2m-o) suggests a critical transition of electric systems. Maintaining a stable power grid requires sophisticated regulation to balance supply and demand, considering complex interactions between meteorological and socio-economic factors and various energy sources.

Considering the urgent needs in electricity management under a changing environment, our DEV analysis has potential for monitoring resilience of power grids at milli-second scale. For example, a real-time grid resilience based on our quantitative warning signal could prevent failures when the power grid approaches a tipping point.

Efficacy of DEV as EWS

Our proposed DEV is a functional EWS, with consistent early warning patterns (e.g., monotonic increase trend) when approaching the tipping point in models and in empirical datasets (Fig. 1-2). Compared to generic EWS, such as autocorrelation (e.g., AR1) and variability (e.g., standard deviation [SD]), autocorrelation and variability had reliable early warning patterns in fold and period-doubling bifurcation (Fig. S1) as reported[9,35]; however, they do not perform well in Neimark-Sacker bifurcation wherein the increasing trend of AR1 is minor and does not reach 1 and the increasing trend of variability is less dramatic (Fig. S1). When applying AR1 and variability indices on empirical cases (Fig. S13), early warning patterns were not always apparent (e.g., Fig. S13b, h, i). This inconsistency might be due to distinct sensitivity of the generic EWS to various types of bifurcation. In addition, some EWS relying on variability, such as SD, are likely more sensitive to existence of process noises (e.g., Fig. S4e and S5e).

It is relevant to discuss theoretical connections between DEV and AR1. Mathematically, if a dynamical system can be approximated by a first-order linear stochastic process (i.e., AR1 process) for the chosen time window, the matrix **J** (eq. 1 in Method) governing the evolution of dynamical system can be formularized as a simple diagonal matrix (i.e., $\mathbf{J}_{AR1}$) with all diagonal elements equal to the estimated AR1. Here, $\mathbf{J}_{AR1}$ was assumed fixed within the analyzed time window, whereas the matrix **J** estimated in DEV can vary within a time window. Obviously, the dominant eigen-value of this matrix $\mathbf{J}_{AR1}$ equals to AR1. Therefore, according to bifurcation theory, AR1 theoretically reaches 1 at the tipping point in fold bifurcation, as suggested[5,9]. However, convergence of AR1 to 1 requires that the dynamical system can be well approximated by first-order stochastic process for the chosen time window. Following the same mathematical reasoning, AR1 shall approach -1 for period-doubling bifurcation because the dominant eigen-value will reach -1 around the tipping point; this was confirmed by our analysis of

Hénon map (Fig. S1). Regardless, the approximation of AR1 process can only obtain a real-valued dominant eigen-value because the estimated AR1 can never be a complex number. Consequently, AR1 cannot be applied to Neimark-Sacker or other types of bifurcations in which the imaging parts of dominant eigen-values are always preserved. Based on this mathematical reasoning, only fold bifurcation can demonstrate obvious critical slowing down (CSD)[5], wherein the current system state becomes very similar with the previous state (i.e., increasing AR1) prior to critical transition. However, CSD may not occur in other types of bifurcation that manifest only minor increases (e.g., Neimark-Sacker bifurcation in Rosenzweig-MacArthur model) or even decreases (e.g., period-doubling bifurcation) in AR1 (Fig. S1). Therefore, from the perspective of bifurcation theory, application of AR1 for detecting critical transition is a special case of DEV.

Limitation of DEV and forward looking

To evaluate the efficacy of DEV on more complex models, we investigated a stochasticity-driven, patch dynamics model, which exhibited no early earning signal (quantified as variance) prior to critical transition[36] (See details in SI texts, *Additional analysis on the meta-population model using multivariate DEV*; Fig. S14a). For such a system with explicit spatial information, we examined whether our DEV approach was effective. In this study, DEV derived from embedding time series of multiple patches (i.e., multivariate DEV; Fig. S14b, c) had a clear early warning signal near the tipping point, but the DEV derived from embedding time series of a single patch (i.e., univariate DEV; Fig. S14d) did not work. This confirmed previous analysis[37] suggesting that explicit spatial information is necessary to detect the EWS of the critical transition originating from strong spatial processes[37]. Multivariate DEV can be applied not only in a dynamical system with explicit spatial information but also in systems with more than one variable, e.g., Hénon map (Fig. S15). Therefore, a more general DEV framework combing both univariate and multivariate DEV highlights a new research direction that may help detect critical transition emerging from diverse mechanisms, e.g., spatial processes; certainly, more detailed investigations are needed for developing EWS in highly spatial structured systems[38]. Therefore, multivariate DEV can be complementary

to other EWS relying on spatial patterns[39,40]. In addition to the issue of spatial processes, we addressed limitations of DEV for ill-posed cases in SI (*Limitations of DEV method in analyzing atypical transitions)*.

The embedding approach has been used to evaluate system stability; however, these studies estimated the dominant eigen-values based on a single time window (i.e., using the whole time series)[24,41]. In the present study, as the standard procedure for EWS estimations, the moving window approach used to compute DEV (Fig. S2) was necessary. Indeed, based on further analyses, the dominant eigen-value derived from the single-time window approach (Fig. S16) could not reveal reliable early warning patterns and failed to identify the period-doubling bifurcation (Fig. S16f). Therefore, the moving window approach is necessary for computation of EWS because some important properties (e.g., nonlinearity[42]) of dynamical systems changed as the system approached the tipping point.

Concluding remarks

In conclusion, the DEV approach developed in this study, for the first time, proposes an empirical EWS with a quantitative threshold to anticipate occurrence of critical transition and identify type of bifurcation. Although DEV efficacy is likely undermined by measurement and process noises, DEV has great potential to effectively anticipate the occurrence and type of critical transition with a more precautionary defined threshold. Because both occurrence condition and bifurcation type can be unambiguously determined, this should enhance real-world management, enabling timely and effective responses to upcoming new regimes.

Methods

Empirical dynamic modeling

According to the theory of dynamical systems, a system can be described as a set of states (e.g., attractor), whose evolution over time is determined by a set of rules (e.g., equations) that describe how the state of attractor changes as a function of interacting variables. Motion on the attractor can be projected onto the coordinate axis of associated variables, forming time series; conversely, time series of the interacting variables can be projected back to the multidimensional state space to recover the attractor[43]. Therefore,

knowing the state and the set of rules that govern the underlying system is equivalent to knowing the time series of all interacting variables. When studying empirical systems, the set of rules is unknown. Furthermore, it's very likely only one or few variables are measured and their interactions are unknown *a priori*. However, it's possible to reconstruct a topologically invariant shadow version of the attractor using time delayed scalar measurements of a single dynamical variable: $X_t = \left(x_t, x_{t-\tau}, \ldots, x_{t-(E-1)\tau}\right)^T$, where x_i are observations at time point i, E is the embedding dimension, and τ is the time lag. This idea, called state space reconstruction (SSR), is based on Sauer, Yorke and Casdagli's extension[44] of Takens' theorem[27] for dynamical systems. An illustration of the SSR concept is available (tinyurl.com/EDM-intro). Interestingly, due to topological invariance, the reconstructed attractor preserves the essential mathematical features of the original dynamical system. Furthermore, SSR facilitates investigating dynamic properties of the system, including interactions (e.g. Jacobian)[45] and stability[24,28], plus transitions between stable and unstable states[42].

Early warning signal based on the dominant eigen-value

Among properties of dynamical systems, a critical issue of practical importance is the ability to identify and predict critical transition. Mathematically, critical transitions are associated with local bifurcations, i.e., qualitative changes in system behavior due to changes in parameter. Bifurcations result from appearance and disappearance of invariant sets due to changes in stability[46] and can be recognized by changed eigen-values of the Jacobian matrix derived from local linear approximation around a fixed point[11] (i.e., local Jacobian).

Critical transitions can be classified according to changes in the dominant eigen-value, λ, of local Jacobian. In general, there are three types of critical transitions/bifurcations: the *fold (tangent)*, the *period-doubling (flip)* and the *Neimark-Sacker (Hopf) bifurcations*[47]. If a discrete system undergoes a fold bifurcation, stable and unstable equilibriums collide and annihilate, or an equilibrium suddenly appears. Fold bifurcation is indicated by the dominant eigen-value reaching Re(λ)=1 and $|\lambda| = 1$. For period-doubling bifurcation, a regularly repeating series of points double in its period

when bifurcation occurs. Consecutive period doublings cause chaos in dynamical systems. The period doubling bifurcation is indicated by the dominant eigen-value reaching Re(λ)=-1 and $|\lambda| = 1$. If a system undergoes a Neimark-Sacker bifurcation, a closed invariant curve appears from an equilibrium, indicated by a pair of conjugated dominant eigen-values with $\mathrm{Im}(\lambda_{1/2}) \neq 0$ reaching $|\lambda_{1/2}| = 1$.

A methodological challenge is then how to estimate local Jacobian in each time point, to track its change through time. In state space, the Jacobian is the local linear approximation of the dynamical system. To reconstruct the Jacobian at point X_N, Eckmann and Euelle (1985) proposed an idea that minimize the squared error, $error^2 = \frac{1}{\#\mathrm{U}} \sum_{X_{i \in \mathrm{U}}} \left\| X_{i+1} - \mathbf{J} X_i - v \right\|^2$, with respect to the coefficients of matrix **J** and some offset vector v, given the set $\mathcal{U}$ of all neighbors of X_N with a distance less than a defined value, ϵ. This basic idea has been adapted in subsequent algorithms[48,49] to calculate local Jacobians and to estimate Lyapunov exponents from observed time series. However, a critical issue of these algorithms is to determine the size of $\mathcal{U}$; if too small, the system is under-represented, the coefficients of matrix **J** cannot be reliably estimated, and algorithms are sensitive to noise. However, if $\mathcal{U}$ is too big, noise becomes less important, but underlying nonlinear dynamics may not be detected[46].

In this study, we estimated the local Jacobian using S-map[28,45], able to overcome problems associated with selecting $\mathcal{U}$ and to account for system nonlinearity. In detail, S-map involves generating an E-dimensional embedding (univariate or multivariate). The state space at time t is given by $X_t = \left(x_t, x_{t-\tau}, ..., x_{t-(E-1)\tau} \right)^T$. For each target time point t_a, the S-map algorithm computes a local linear model $\boldsymbol{C}$ that predicts the future value $Y_{t_a+\tau}$ using the vector X_{t_a} from the reconstructed state space. That is,

$$Y_{t_a+\tau} = C_0 + \sum_{j=1}^{E} C_j \, x_{t_a-(j-1)\tau}$$

The linear model is fitted to other vectors in the state space. However, in contrast to linear regression models, linear approximation in S-map is done only locally by giving greater weighting to points close to the target point, X_{t_a}. The model $\boldsymbol{C}$ is the singular

value decomposition (SVD) solution to the equation,

$$B = \boldsymbol{A} \cdot C$$

where B is an n-dimensional vector (n is the number of observations) of the weighted future values of Y_{t_i} for each historical point, t_i, given by

$$B_i = w\left(\left\|X_{t_i} - X_t\right\|^2\right) Y_{t_i+\tau}$$

and $\boldsymbol{A}$ is then $n \times E$ dimensional matrix given by

$$A_{ij} = w\left(\left\|X_{t_i} - X_t\right\|^2\right) x_{t_i-(j-1)\tau}$$

The weighting function w is defined by

$$w(d) = \exp\left(-\frac{\theta d}{\bar{d}}\right)$$

where $\|\cdot\|^2$ denotes the Euclidean distance and $\bar{d}$ is the average distance between Y_{t^*} and all other vectors on the attractor. The extent of this weighting is tuned by the nonlinear parameter $\theta \geq 0$. Note that the model C is separately calculated for each time point, t^*. Thus, C potentially differs for each time point in the series. Coefficients of the local linear model provided by $\boldsymbol{C}$ are an approximation of local Jacobians[24,45] that can be used as a proxy of the interaction strength between embedded variables.

The original algorithm proposed in Deyle et al.[20] aimed to estimate local Jacobians using multivariate time series of interacting variables. However, these algorithms can be used for embedded time series from a single variable, following the concept of lagged coordinate embedding (i.e., univariate embedding). Here, we aimed to estimate the coefficients of $X_{t+\tau} = \mathbf{J}X_t + v$ with respect to matrix **J** and offset vector v. Since the reconstructed state space is a delay embedding space of a univariate time series, almost all elements of the Jacobian, **J**, are zero, except the lower-off diagonal, which are unity, and except the first row, which contains the non-trivial linear approximation. The same argument holds for the offset vector v. Here, the linearized dynamics read

435 $$\begin{pmatrix} x_{t+\tau} \\ x_t \\ \vdots \\ x_{t-(E-2)\tau} \end{pmatrix} = \begin{pmatrix} j_{11} & \cdots & \cdots & j_{1E} \\ 1 & 0 & \cdots & 0 \\ 0 & \ddots & \ddots & \vdots \\ \cdots & 0 & 1 & 0 \end{pmatrix} \begin{pmatrix} x_t \\ \vdots \\ x_{t-(E-2)\tau} \\ x_{t-(E-1)\tau} \end{pmatrix} + \begin{pmatrix} v_1 \\ 0 \\ \vdots \\ 0 \end{pmatrix} \quad (1)$$

436 Following the S-map algorithm, matrix **J** of parameters $j_{11}, \ldots, j_{1E}$ can be calculated
437 as the associated S-Map coefficients[24,45]. Because **J** is evaluated at each time point (i.e.,
438 local Jacobian **J**(t)), it is time-varying. With the Jacobians, it is possible to calculate the
439 dominant eigen-value for each local Jacobian through time and evaluate the system's
440 local Lyapunov stability (as an EWS of critical transition), and can further identify the
441 type of critical transition (see Box 1). As the dominant eigen-value changes through time,
442 we named this indicator Dynamical Eigen-Value (DEV). More importantly, DEV
443 anticipates occurrence and type of critical transition (Fig. S2).

444

445 *Model data*

446 To demonstrate the efficacy of the DEV approach, we analyzed three representative
447 models with disparate types of critical transition, including Noy-Meir model (fold
448 bifurcation), Hénon map (period doubling bifurcation), as well as a discrete version of the
449 Rosenzweig-MacArthur model (Neimark-Sacker bifurcation). In these model simulations,
450 bifurcation parameters were chosen to demonstrate critical transitions. For these three
451 models, equations are:

452 The Noy-Meir model[50] is described by:

453 (3) $$N_{t+1} = N_t \exp\left(0.75 - 0.1N_t\right) - F\frac{N_t^2}{N_t^2 + 0.75^2} + \omega_t \zeta N_t$$

454 The bifurcation parameter F was linearly increased from 0 to 2 throughout the whole
455 simulated time series.

456 The Hénon map[51] reads as

457 (1) $$x_{t+1} = 1 - ax_t^2 + y_t + \omega_t \zeta x_t$$

(2) $y_{t+1} = 0.3x_t$

The bifurcation parameter a was linearly increased from 0.1 to 0.4 throughout the whole simulated time series.

Finally, the Rosenzweig-MacArthur model[52] reads as

(4) $$x_{t+1} = (1+l)\,x_t - 4x_t^{\,2} - \frac{x_t y_t}{1+0.5x_t} + \omega_t \zeta x_t$$

(5) $$y_{t+1} = -2y_t + \frac{6x_t y_t}{1+0.5x_t}$$

The bifurcation parameter l was linearly increased from 3.48 to 3.78 throughout the whole simulated time series. Following Dakos et al.[42], we used a stochastic modeling framework, applying process noise on the state variable (x_t or N_t) based on Gaussian white noise, ωx_t. Noise was multiplied by ζ as ζx_t or ζN_t. Consequently, the standard deviation of the noise is ζ times the value of the previous time step.

For each model, we generated the time series. First, we chose fixed parameters (i.e., those other than the tuning bifurcation parameter) by determining the equilibrium in the absence of noise with the bifurcation parameter at the initial value. Subsequently, time series variables at equilibrium were the initial values for modeling the stochastic system, thereby avoiding the burn-in period. Then, a time series was generated while gradually changing the bifurcation parameter. For each simulation, a time series of 10000 points was generated, as reported[28].

Empirical data

The DEV approach (explained in the DEV analysis section below) was applied on five empirical data sets: (1) cyanobacteria under light stress in a microcosm[32], (2) phonation onset under increasing flow rate, (3) cytosolic ATP dynamics in living plant tissues under progressing hypoxia [53], (4) calcium carbonate ($CaCO_3$) level in sediments before the end of last greenhouse Earth [54], and (5) bus voltage frequency before the North Western US power grid failure in 1996[55].

484

485 Cyanobacteria under light stress

486 We re-analyzed the response of a cyanobacteria population in chemostats to dilution
487 events under a regime of gradually increasing light intensity[32]. Population density was
488 determined as the light attenuation coefficient calculated from continuous measurements
489 of outgoing light intensity. In total, this time series included 7784 data points spanning
490 28.86 days, with time interval equal to 0.0035 day (5 min). The overall time series
491 consisted of six segments separated by dilution events (Fig. 2a and Table S1). Since
492 dilution events were not part of the population dynamics, only time series segments were
493 analyzed after recovery from the previous dilution event and before undergoing the new
494 dilution event. Because the shortest continuous segment (the one prior to dilution event
495 P2) was 250 time points long (~ 1 day), to be consistent for all dilution events, only the
496 last 250 data points were used before each dilution event when analyzing all segments
497 (P1-P6; in total 6*250 = 1500 data points).

498

499 Phonation onset under increasing flow

500 Phonation onset (i.e., onset of vocal fold oscillation) is regarded as a Hopf
501 bifurcation in the framework of dynamical systems[56]. To experimentally realize the
502 phonation onset using a physical replica the vocal folds, an EPI (i.e., "epithelium") model
503 was constructed following an established procedure[57]. In accordance with vocal fold
504 physiology, the EPI model had a body-cover structure. The cover layer was based on an
505 extremely flexible superficial layer of lamina propria (SLLP), covered by a thin
506 epithelium. The SLLP layer was attached to the body layer by a ligament layer. Individual
507 layers with varying stiffness and strength were produced with silicone. With the detailed
508 multi-layer structure, the EPI model oscillated with a pronounced convergent-divergent
509 motion, resembling real vocal-fold oscillations.

510 The experimental set-up to realize flow-induced oscillations of the vocal fold model
511 has been reported[58]. In this experiment, no supraglottal tube was attached. The subglottal
512 pressure was measured by a pressure transducer (Differential pressure transducer, PDS
513 70GA, Kyowa; Signal conditioner, CDV 700A, Kyowa), located 2 cm upstream of the

514 vocal fold model, and recorded with 44 kHz sampling rate. During the experiment of
515 phonation onset, the flow-rate was slowly increased until the vocal folds started to
516 oscillate. From this experiment, we obtained time series data including 7501 data points,
517 spanning of 0.375 second overall, with time interval equal to $5*10^{-5}$ second (Fig. 2d and
518 Table S1).
519
520 Cellular energy status under hypoxia
521 The data are dynamics of ATP concentrations in the cytosol of living leaf cells over
522 time, measured by fluorimetry using an intracellular FRET-sensor that responds to
523 $MgATP^{2-}$. In the dark, leaves respire and gradually deplete ambient oxygen within a
524 sealed compartment, creating cellular hypoxia, and decreasing energy charge. The ATP
525 remained relatively stable while oxygen was gradually depleted, then suddenly dropped
526 (Fig. 2g). Interestingly, this drop appeared to occur before the oxygen concentration was
527 limiting for the mitochondrial respiratory chain (responsible for most cellular ATP
528 production). How ATP stabilization and collapse are modulated mechanistically in the
529 living cell is unknown.
530 The data represented the fluorescent readout of a genetically-encoded fluorescent
531 protein-based Förster Resonance Energy Transfer (FRET) sensor that indicated ambient
532 concentrations of the biological energy carrier molecule ATP (i.e., its dominant
533 bioavailable form in the cell, $MgATP^{2-}$)[59]. The sensor (ATeam 1.03-nD/nA) consists of a
534 blue fluorescent protein (the CFP derivative mseCFP), a yellow fluorescent protein (the
535 YFP derivative cp178-mVenus) and an ATP-binding domain (ε-subunit from *Bacillus*
536 *subtilis* F_oF_1-ATP synthase)[59]. The more $MgATP^{2-}$ is present in the direct environment of
537 the protein, the higher the FRET; therefore, the fluorescence emission of the YFP
538 acceptor increased, while that of the CFP donor simultaneously decreased. For the
539 measurement, the sensor protein is genetically expressed in the cytosol of leaves of the
540 model plant *Arabidopsis thaliana* (5- to 6-weeks-old)[60]. Leaf slices (30 mg fresh weight)
541 were placed in a single well of a 96-well multititer plate[53]. The well was filled with
542 medium and sealed with a transparent, air-tight film to prevent oxygen diffusion. In the
543 dark, the tissue respires available oxygen, causing gradual hypoxia. After sealing the well
544 and starting fluorescence recording, the sensor indicated a slight gradual decline of

545 cytosolic $MgATP^{2-}$ until the FRET ratio suddenly decreased, indicating cytosolic
546 $MgATP^{2-}$ concentrations had collapsed (Fig. 2d). Leaf tissue fluorescence was measured
547 every 40 s, background fluorescence was subtracted for isolating the sensor signal, and
548 the fluorescence emission ratio YFP/CFP was calculated. Five biological replicates were
549 measured with similar observations, and the experiment was repeated twice. The dataset
550 analyzed here was recently reported[53], and we used time series data including 271 data
551 points, spanning an overall of 3 min, with time interval equal to 0.011 min (Fig. 2g and
552 Table S1).
553
554 Calcium carbonate in the end of greenhouse Earth
555 We re-analyzed the calcium carbonate ($CaCO_3$) time series associated with the end
556 of greenhouse Earth[54] that marked the transition of an ice-cap free Earth to an Earth with
557 polar ice-caps. In this study, the time series had an increase in autocorrelation while
558 approaching the climate shift. In total, this time series includes 462 data points, spanning
559 an overall of 5.9 million years with time interval equal to 0.013 million years. (Fig. 2j and
560 Table S1).
561
562 Bus voltage frequency before power grid failure
563 We analyzed bus voltage frequency data measured before the Western Interconnect
564 Blackout of August 1996. The time series consist of ~10 min of measurements at a
565 sampling rate of $\Delta t = 0.02415$s from the Bonneville Power Administration territory, until
566 the point of separation. This time series exhibited critical fluctuation approaching the
567 point of blackout[61]. For our study, data were prepared as in a previous study[61]. In total,
568 this time series included 23393 data points, spanning an overall of 565 seconds with time
569 interval equal to 0.024 second. (Fig. 2m and Table S1).
570
571 *Dynamical Eigen-Value (DEV) analysis*
572 The most critical step for the DEV approach is to reconstruct the attractor. As system
573 dynamics may change through time, we employed a windowing approach, instead of
574 estimating the Jacobians using the whole time series, as reported.[24] Thus, a proper
575 window size, *w*, (i.e., length of time series segment for estimating DEV) needs to be

chosen for each time series analysis, to best describe the associated dynamics of the system. In addition, best embedding dimension, E, and time lag, τ, need to be estimated.

As in previous publications applying S-map, we screened for the parameter orchestration resulting in the best performance (i.e., S-map prediction skill[62]). To determine the optimal window size for computation, we screened various window sizes; for each, we evaluated S-map skill (predictability, ρ) for various combinations of embedding dimensions E (1 to 12) and time lags τ (1 to 12) and obtained the highest ρ (ρ_{max}). While searching the optimal window size, for simplifying the calculation, we chose $\theta = 0$ in S-map, as recommended.[63] When $\theta = 0$, S-map is equivalent to an autoregressive model of order E[64]. The optimal window size (w) close to the plateau is determined visually, beyond which increasing the window size leads to very minor improvements in predictability (Fig. S2a). Considering the paucity of time series data and avoiding the risk of overfitting, we chose a window size close to the plateau phase. The best E and τ associated with the optimal window size resulting in best ρ were used throughout the analysis. Then, sensitivity analysis for various E, τ, and w should be done to ensure results are robust. Selected parameters for the state space reconstruction of each dataset are summarized in Table S1.

After determining w, E, and τ, we proceeded to estimate the time series of Jacobian for the window segment (Fig. S2b, c & d). To account for changing nonlinearity of the reconstructed attractor [42], for each time series segment defined by the moving window, S-map analyses were run for various θ (0 to 2.5); the best θ giving the best S-map forecast skill was chosen. After obtaining the time series of Jacobian, we subsequently calculated the dominant eigen-value at each time point within the window. Then, we averaged all eigen-values derived in the time window as our DEV indicator. The averaging process smoothed out the uncertainty of estimating DEV at each time point; furthermore, the averaged DEV indicated the vulnerability to critical transition for that region of attractor. Finally, moving the window forward and repeating the calculation for every time step, we obtained the time series of DEV. Absolute of DEV approaching 1 was indicative of critical transition. Using time series segments of the chosen window size, we consecutively estimated the early warning signals. The signals were reported and matched to the time index associated with the last point of the window. However, extrapolation

607 can be done using a simple linear regression between DEV versus time (Fig. 2), to
608 visualize and anticipate the occurrence of critical transition. If DEV approaches 1
609 nonlinearly, a nonlinear curve can be fit.

610

611 *Sensitivity of DEV approach to stochasticity*

612 Noise (process and observation error) may undermine DEV efficacy. Thus, we
613 examined effects of noise on our three mathematical models. To create observation error,
614 after generating a time series, observation error was added by substituting each time point
615 x_t by a normally-distributed random value with mean x_t and standard deviation φ, where φ
616 determined the level of observation noise. The process error was intrinsically included in
617 our stochastic models. To increase process noise, we increased the parameter ζ (see the
618 section of Model data).

619 For a given combination of process noise and observation error (see Supplementary
620 Figs. S4-7 for combinations), 100 simulations were run for each model. For each run, the
621 DEV estimates at the first window and the window immediately prior to bifurcation were
622 used for further analysis. Consequently, we demonstrated both *quantitative* and
623 *qualitative* properties of the DEV as an EWS. Mathematically, the absolute value of the
624 dominant eigen-value is 1 at bifurcation; therefore, the estimated DEV should be close to
625 1, too, to be a robust *quantitative* indicator. Furthermore, eigen-values are expected to
626 increase prior to bifurcation. Thus, ΔDEV, defined as the difference between DEV prior
627 to bifurcation and DEV at the initial phase of the simulation, was calculated to
628 demonstrate that DEV was a *qualitative* EWS.

629 Note that for the Rosenzweig-MacArthur model, even intermediate level of process
630 noise resulted in breakdown of the system (infinite values); thus, only limited level of
631 process noise can be examined (Fig. S6).

632

633 *Comparison with AR1 and variance*

634 For comparative purposes, all data were also analyzed using the two most commonly
635 used resilience indicators, autocorrelation and variance. We estimated 1-lag

636 autocorrelation (AR1) as the Pearson correlation for lagged time series at one point, and
637 variance as the standard deviation (SD). To make results comparable, the same window
638 size as that for the DEV approach was used. Prior to analysis, linear trends in the time
639 series segment were removed using simple regression.

640

641 *Computation*

642 All analyses were done with R (ver. 3.1.2). The S-map analyses were implemented
643 using the rEDM, and AR1 and variance were computed using the built-in functions in R.
644 All analytical procedures and R codes noted above are documented (https://github.com/f-
645 grzi/DEV).

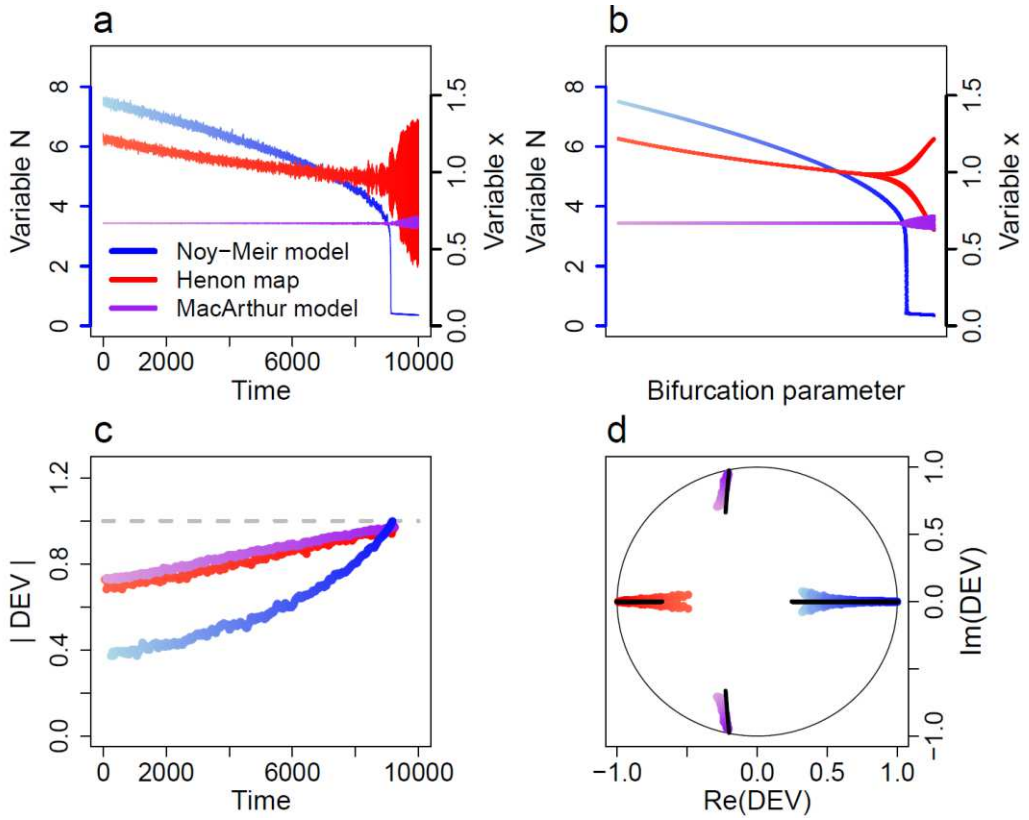

646

647 **Figure 1. Efficacy of Dynamical Eigen-Value (DEV) method as early warning signal**
648 **indicating critical transitions in the three mathematical models.** (a) Exemplary time
649 series of the Noy-Meir model (blue), Hénon map (red), and Rosenzweig-MacArthur
650 model (purple). (b) The bifurcation diagram illustrates effects of changing bifurcation
651 parameters (See Supplementary Table S1 for parameter values) on the averaged variable
652 states calculated from moving windows. (c) The estimated |DEV| increase over time and
653 approach 1 at the bifurcation point (shown in panel a and b). (d) The classification of
654 bifurcation types based on |DEV| estimates on the complex plane (*sensu* Box 1). The
655 |DEV| estimates move from interior of the unit circle toward the border through time,
656 signaling critical transition; the color gradients from light to dark represent time
657 progression from initial time to the time right before critical transitions. Note that for
658 each eigen-value with a nonzero imaginary part a pair of conjugated eigen-values exist
659 and show mirror symmetry on the complex plane. In panel (d), the minor values in the
660 imaginary axis appear in the Noy-Meir model (blue) and Hénon map (red), owing to
661 process noises included in models. Black lines within the circle labeled the theoretical
662 dominant eigen-values.

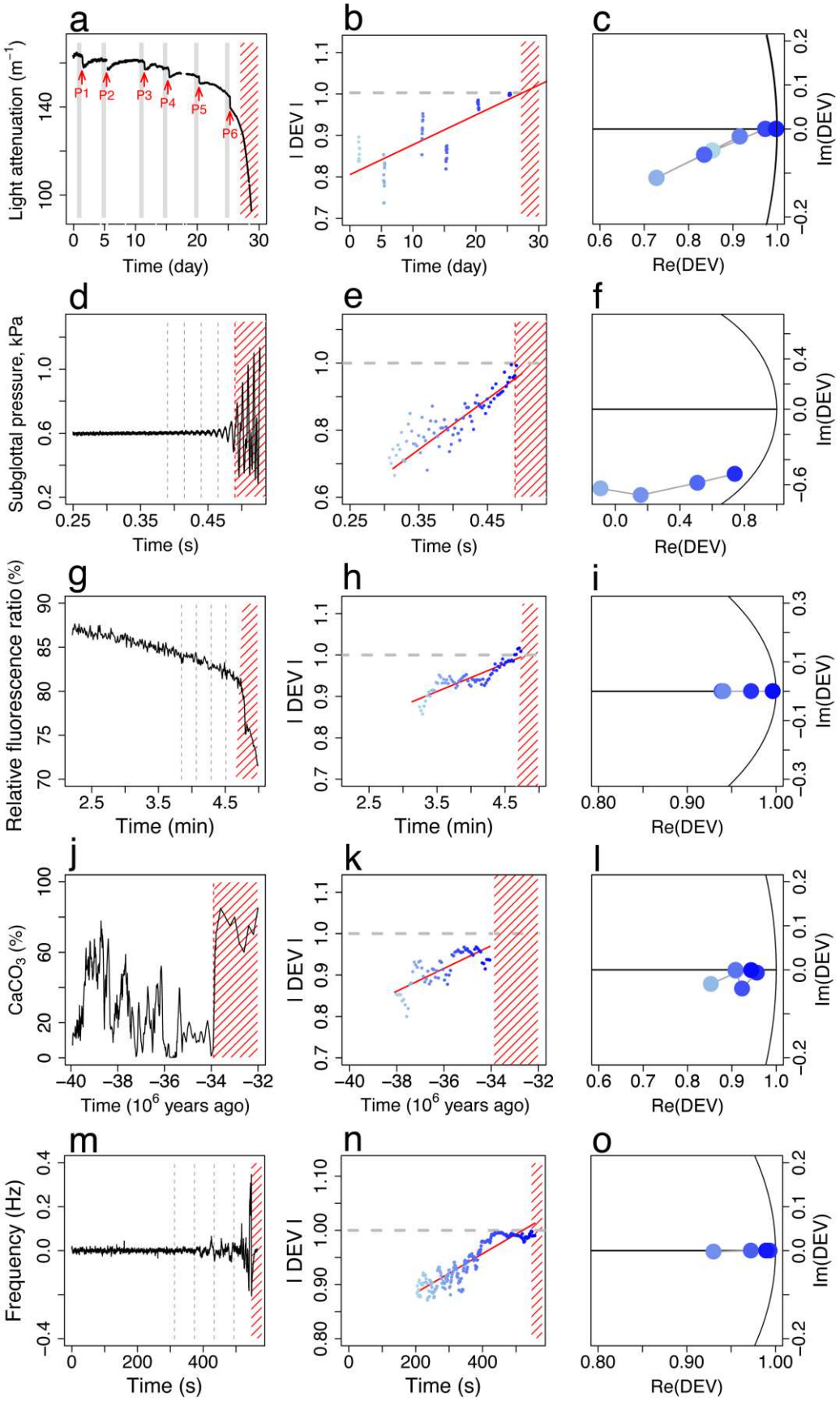
a
b
c
d
e
f
g
h
i
j
k
l
m
n
o
Light attenuation (m^{-1})
P1
P2
P3
P4
P5
P6
Time (day)
I DEV I
Re(DEV)
Im(DEV)
Subglottal pressure, kPa
Time (s)
Relative fluorescence ratio (%)
Time (min)
CaCO$_3$ (%)
Time (10^6 years ago)
Frequency (Hz)

663

Figure 2. Empirical evaluations showing that |DEV|s can be early warning signal for critical transition and indicate type of bifurcation. |DEV|s signal: fold-bifurcation in a microcosm experiment of a cyanobacteria population undergoing dilution perturbations and increasing light stress (a-c); Neimark-Sacker-bifurcation in an experiment of voice onset under increasing flow rate (measured subglottal pressure) (d-f); fold-bifurcation in an *in vivo* biosensing experiment of cytosolic ATP at progressing hypoxia (g-i); fold-bifurcation in climate data of $CaCO_3$ abundance in sediments from the end of the last greenhouse earth (j-l); fold-bifurcation in electricity data of "1996 Western North America blackouts" (m-o). Panels (a), (d), (g), (j), and (m) illustrate time series data; the red dashed area delineates the regime after critical transition. In (a), arrows indicate external perturbations, and we estimated |DEV|s from the 250 data points (~1 day) before each perturbation (gray area). Panels (b), (e), (h), (k), and (n) illustrate the time series of estimated |DEV|; the red lines derived from the linear regression of |DEV| versus time, and the |DEV| value of 1 (grey dash line) indicates the bifurcation point. Panels (c), (f), (i), (l), and (o) indicate type of bifurcation. For better visualization, in panel (c), we averaged |DEV| estimates associated with the same perturbations event; while in panels (f), (i), (l), and (o), |DEV| estimates are averaged in time intervals prior to the bifurcation (delineated by dashed lines in d, g, j, and m). The color gradients from light to dark present time progression from initial time to the time right before critical transitions.

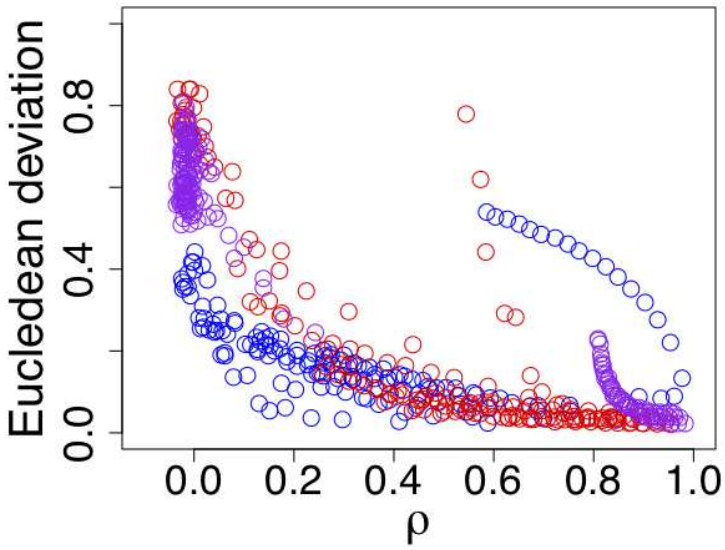

Figure 3. Uncertainty of DEV as a function of predictability (ρ) for the mathematical models with different combinations of noises. Results of the Noy-Meir model (blue), Hénon map (red), and Rosenzweig-MacArthur model (purple) under a specific combination of observation noise and process error. Each curve was obtained by plotting the uncertainty (defined as the Euclidean distance between the analytic eigen-value and the estimated DEV in complex plane) as a function of predictability (ρ) measured within each moving window in the DEV analysis. For all combinations of noises, the uncertainty decreased with increasing one-step forward predictability. In addition, there was no noticeable difference between the analytically solved and DEV derived eigen-value when the predictability was high (e.g., ρ>0.8). Thus, the one-step forward predictability could be used to evaluate the reliability of DEV as quantitative early warning signal.

Box 1. Information about bifurcations.

Critical transition is initiated from local bifurcation, which results from destabilization of the dynamical system accompanied with appearance and disappearance of invariant sets[47] (Box Table 1). Mathematically, bifurcation was recognized by changes in the dominant eigen-value, λ, of the Jacobian matrix, $\mathbf{J}$. The Jacobian matrix $\mathbf{J}$ of a n-dimensional dynamical system is defined as

$$\mathbf{J} = \begin{pmatrix} \frac{\partial f_1}{\partial x_1} & \frac{\partial f_1}{\partial x_2} & \cdots & \frac{\partial f_1}{\partial x_n} \\ \frac{\partial f_2}{\partial x_1} & \frac{\partial f_2}{\partial x_2} & \cdots & \frac{\partial f_2}{\partial x_n} \\ \vdots & \ddots & \ddots & \vdots \\ \frac{\partial f_n}{\partial x_1} & \frac{\partial f_n}{\partial x_2} & \cdots & \frac{\partial f_n}{\partial x_n} \end{pmatrix}$$

, where n functions $f_1\left(x_1, \ldots, x_n\right), \ldots, f_n\left(x_1, \ldots, x_n\right)$ describe the dynamics of n variables $x_1, \ldots, x_n$, respectively. Based on the dominant eigen-values of Jacobian matrices, three types of bifurcation, including the *fold (*or *saddle-node)*, the *period-doubling* (or *flip*) and the *Neimark-Sacker (*or *Hopf)* bifurcations[47], can be explicitly distinguished in complex plane (Box Table 1 and Box Figure 1).

To infer the dominant eigen-values at each time point, it is well known that local Jacobian matrices can be estimated from time series by reconstructing the local linear approximations of the dynamics in state space (see Methods). Because time series data are discrete, the absolute value of the dominant eigen-value reaches 1 (i.e., $|\lambda| \rightarrow 1$) at the bifurcation point in all types of bifurcations. Note that the time series data simulated from continuous systems, such as differential equations, are also discrete as they are solved numerically. The properties of dominant eigen-values inferring the bifurcations in continuous systems are described in Fig. S1.

718 **Box Table 1: System change and dominant eigen-value of different bifurcation types**

Bifurcation type	*Change in invariant sets*	*Dominant eigen-value, λ*
Fold	Appearance or disappearance of stable and unstable equilibria	$\mathrm{Im}(\lambda)=0$ and $\mathrm{Re}(\lambda) \to 1$
Period-doubling	Doubling the periods of limit cycles	$\mathrm{Im}(\lambda)=0$ and $\mathrm{Re}(\lambda) \to -1$
Neimark-Sacker	Appearance of a closed invariant curve	$\mathrm{Im}(\lambda_{1/2})\neq 0$ and $\lvert\lambda_{1/2}\rvert \to 1$

719

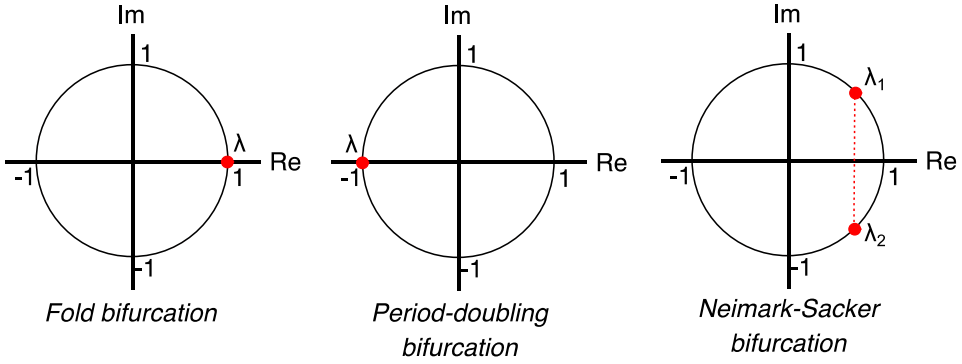

720

721 **Box Figure 1: Schematic illustration of the dominant eigen-value in complex plane**
722 **at the bifurcation point for three types of bifurcation.**

723

Acknowledgments: This work was supported by the National Center for Theoretical Sciences, National Taiwan University, Academia Sinica, Foundation for the Advancement of Outstanding Scholarship, and the Ministry of Science and Technology, Taiwan (to C.H.H). Comments from Lin-Yun Chiao on an earlier draft and English editing by J. Kastelic improved the manuscript. We thank Stephan Wagner (Cologne, Germany) for the original recording of published data on cellular energy status at hypoxia analyzed in this work.

Statement of authorship:

C.H.H., F.G., and A.T. conceived the research idea; F.G. and C.W.C developed the methods and analyzed the models and data, with help from V.D., C.H.H., A.T., and E.H.V; V.D., M.H., O.K., M.S., and I.T.T provided data; C.W.C., C.H.H., F.G., and A.T. wrote the manuscript with comments from all co-authors.

Competing interests: The authors declare no competing interests.

Running title: Anticipate occurrence and type of critical transitions

Keywords: Critical transition; tipping point; Early warning signal; Bifurcation; Dynamical system

The type of article: Article

Number of words in abstract: 149

Number of words in main text: 3456

Number of cited references: 64

Number of tables & figures: 3 figures and 1 box

Data availability:

Data availability is described in Table S2. Individual dataset is available upon request to the data owner, as listed in the Table S2.

Code availability: Documentation of all analytical procedures provided as R codes are available from Github: https://github.com/f-grzi/DEV.

References

1 Scheffer, M., Carpenter, S., Foley, J. A., Folke, C. & Walker, B. Catastrophic shifts in ecosystems. *Nature* **413**, 591-596 (2001).

2 van de Leemput, I. A. *et al.* Critical slowing down as early warning for the onset and termination of depression. *Proceedings of the National Academy of Sciences* **111**, 87-92 (2014).

3 Haldane, A. G. & May, R. M. Systemic risk in banking ecosystems. *Nature* **469**, 351-355 (2011).

4 Wang, R. *et al.* Flickering gives early warning signals of a critical transition to a eutrophic lake state. *Nature* **492**, 419-422 (2012).

5 Dakos, V. *et al.* Slowing down as an early warning signal for abrupt climate change. *Proceedings of the National Academy of Sciences* **105**, 14308-14312 (2008).

6 Scheffer, M. *et al.* Anticipating critical transitions. *Science* **338**, 344-348 (2012).

7 Topaz, C. M., D'Orsogna, M. R., Edelstein-Keshet, L. & Bernoff, A. J. Locust dynamics: behavioral phase change and swarming. *PLoS Comp. Biol.* **8**, e1002642 (2012).

8 Clark, P. U., Pisias, N. G., Stocker, T. F. & Weaver, A. J. The role of the thermohaline circulation in abrupt climate change. *Nature* **415**, 863-869 (2002).

9 Scheffer, M. *et al.* Early-warning signals for critical transitions. *Nature* **461**, 53-59 (2009).

10 Nes, Egbert H. v. & Marten Scheffer. Slow recovery from perturbations as a generic indicator of a nearby catastrophic shift. *The American Naturalist* **169**, 738-747 (2007).

11 Strogatz, S. H. *Nonlinear Dynamics and Chaos: With Applications to Physics, Biology, Chemistry, and Engineering*. 2nd edn, (CRC Press, 2015).

12 Wissel, C. A universal law of the characteristic return time near thresholds. *Oecologia* **65**, 101-107 (1984).

13 Dakos, V., van Nes, E. H., D'Odorico, P. & Scheffer, M. Robustness of variance and autocorrelation as indicators of critical slowing down. *Ecology* **93**, 264-271 (2012).

14 Kéfi, S., Dakos, V., Scheffer, M., Van Nes, E. H. & Rietkerk, M. Early warning signals also precede non-catastrophic transitions. *Oikos* **122**, 641-648 (2013).

15 Dakos, V., Carpenter, S. R., Nes, E. H. v. & Scheffer, M. Resilience indicators: prospects and limitations for early warnings of regime shifts. *Philosophical Transactions of the Royal Society B: Biological Sciences* **370**, 20130263 (2015).

16 Weinans, E., Quax, R., van Nes, E. H. & Leemput, I. A. v. d. Evaluating the performance of multivariate indicators of resilience loss. *Scientific Reports* **11**, 9148 (2021).

17 Bury, T. M. *et al.* Deep learning for early warning signals of tipping points. *Proceedings of the National Academy of Sciences* **118**, e2106140118 (2021).

18 Scheffer, M., Carpenter, S. R., Dakos, V. & van Nes, E. H. Generic Indicators of Ecological Resilience: Inferring the Chance of a Critical Transition. *Annual Review of Ecology, Evolution, and Systematics* **46**, 145-167 (2015).

19 Kuznetsov, Y. A. *Elements of applied bifurcation theory*. Vol. 112 (Springer Science & Business Media, 2013).

20 Deyle, E. R., May, R. M., Munch, S. B. & Sugihara, G. Tracking and forecasting ecosystem interactions in real time. *Proc. Royal Soc. B* **283**, 20152258 (2016).
21 Cenci, S. & Saavedra, S. Uncertainty quantification of the effects of biotic interactions on community dynamics from nonlinear time-series data. *J R Soc Interface* **15**, 20180695 (2018).
22 Ye, H. *et al.* Equation-free mechanistic ecosystem forecasting using empirical dynamic modeling. *Proc. Natl. Acad. Sci. U.S.A.* **112**, E1569-E1576 (2015).
23 Ives, A. R. & Dakos, V. Detecting dynamical changes in nonlinear time series using locally linear state-space models. *Ecosphere* **3**, art58 (2012).
24 Ushio, M. *et al.* Fluctuating interaction network and time-varying stability of a natural fish community. *Nature* **554**, 360-363 (2018).
25 Chang, C.-W., Ushio, M. & Hsieh, C.-h. Empirical dynamic modeling for beginners. *Ecological Research* **32**, 785-796 (2017).
26 Sugihara, G. & May, R. M. Nonlinear forecasting as a way of distinguishing chaos from measurement error in time series. *Nature* **344**, 734-741 (1990).
27 Takens, F. in *Dynamic systems and turbulence Lecture Notes in Mathematics* (eds D. A. Rand & L. S. Young) 366-381. (Springer-Verlag, 1981).
28 Cenci, S. & Saavedra, S. Non-parametric estimation of the structural stability of non-equilibrium community dynamics. *Nature Ecology & Evolution* **3**, 912-918 (2019).
29 Golubitsky, M., Stewart, I. & Schaeffer, D. G. *Singularities and Groups in Bifurcation Theory: Volume II*. Vol. 69 (Springer Science & Business Media, 2012).
30 Chang, C.-W. *et al.* Reconstructing large interaction networks from empirical time series data. *Ecology Letters* **00**, 1-12 (2021).
31 Roda, W. C., Varughese, M. B., Han, D. & Li, M. Y. Why is it difficult to accurately predict the COVID-19 epidemic? *Infectious Disease Modelling* **5**, 271-281 (2020).
32 Veraart, A. J. *et al.* Recovery rates reflect distance to a tipping point in a living system. *Nature* **481**, 357-359 (2012).
33 Sun, N., Youle, R. J. & Finkel, T. The mitochondrial basis of aging. *Molecular Cell* **61**, 654-666 (2016).
34 Nunnari, J. & Suomalainen, A. Mitochondria: In Sickness and in Health. *Cell* **148**, 1145-1159 (2012).
35 Dakos, V. *et al.* Methods for detecting early warnings of critical transitions in time series illustrated using simulated ecological data. *PLoS ONE* **7**, e41010-e41010 (2012).
36 Hastings, A. & Wysham, D. B. Regime shifts in ecological systems can occur with no warning. *Ecology Letters* **13**, 464-472 (2010).
37 Carpenter, S. R. & Brock, W. A. Early warnings of regime shifts in spatial dynamics using the discrete Fourier transform. *Ecosphere* **1**, art10 (2010).
38 Kramer, M. A. *et al.* Human seizures self-terminate across spatial scales via a critical transition. *Proceedings of the National Academy of Sciences* **109**, 21116-21121 (2012).
39 Dakos, V., van Nes, E. H., Donangelo, R., Fort, H. & Scheffer, M. Spatial correlation as leading indicator of catastrophic shifts. *Theoretical Ecology* **3**, 163-

174 (2010).
40 Kéfi, S. *et al.* Early warning signals of ecological transitions: methods for spatial patterns. *PLoS ONE* **9**, e92097 (2014).
41 Cenci, S., Sugihara, G. & Saavedra, S. Regularized S-map for inference and forecasting with noisy ecological time series. *Methods in Ecology and Evolution* **10**, 650-660 (2019).
42 Dakos, V., Glaser, S. M., Hsieh, C. H. & Sugihara, G. Elevated nonlinearity as an indicator of shifts in the dynamics of populations under stress. *J. R. Soc. Interface.* **14**, 20160845 (2017).
43 Deyle, E. & Sugihara, G. Generalized theorems for nonlinear state space reconstruction. *PLoS ONE* **6**, e18295 (2011).
44 Sauer, T., Yorke, J. A. & Casdagli, M. Embedology. *Journal of Statistical Physics* **65**, 579-616 (1991).
45 Deyle, E. R., May, R. M., Munch, S. B. & Sugihara, G. Tracking and forecasting ecosystem interactions in real time. *Proc. R. Soc. Lond. B. Biol. Sci.* **283**, 20152258 (2016).
46 Kantz, H. & Schreiber, T. *Nonlinear time series analysis*. 2nd edn, 369. (Cambridge University Press, 2010).
47 Kuznetsov, Y. A. *Elements of Applied Bifurcation Theory*. (Springer, 2004).
48 Sano, M. & Sawada, Y. Measurement of the Lyapunov Spectrum from a Chaotic Time Series. *Phys. Rev. Lett.* **55**, 1082-1085 (1985).
49 Chereskin, T. K. & Trunnell, M. Correlation scales, objective mapping, and absolute geostrophic flow in the California Current. *Journal of Geophysical Research* **101**, 22619-22629 (1996).
50 Noy-Meir, I. Stability of grazing systems: An application of predator-prey graphs. *Journal of Ecology* **63**, 459-481 (1975).
51 Hénon, M. in *The Theory of Chaotic Attractors* (eds Brian R. Hunt, Tien-Yien Li, Judy A. Kennedy, & Helena E. Nusse) 94-102. (Springer New York, 1976).
52 Rosenzweig, M. L. & MacArthur, R. H. Graphical representation and stability conditions of predator-prey interactions. *The American Naturalist* **97**, 209-223 (1963).
53 Wagner, S. *et al.* Multiparametric real-time sensing of cytosolic physiology links hypoxia responses to mitochondrial electron transport. *New Phytol.* **224**, 1668-1684 (2019).
54 Dakos, V. *et al.* Slowing down as an early warning signal for abrupt climate change. *Proc. Natl. Acad. Sci. USA* **105**, 14308–14312 (2008).
55 Council, W. S. C. Western Systems Coordinating Council disturbance report for the power system outages that occurred on the Western Interconnection on July 2, 1996 and July 3, 1996. (1996).
56 Mergell, P., Herzel, H., Wittenberg, T., Tigges, M. & Eysholdt, U. Phonation onset: Vocal fold modeling and high-speed glottography. *The Journal of the Acoustical Society of America* **104**, 464-470 (1998).
57 Murray, P. R. & Thomson, S. L. Vibratory responses of synthetic, self-oscillating vocal fold models. *The Journal of the Acoustical Society of America* **132**, 3428-3438 (2012).
58 Shimamura, R. & Tokuda, I. T. Effect of level difference between left and right

vocal folds on phonation: Physical experiment and theoretical study. *The Journal of the Acoustical Society of America* **140**, 3393-3394 (2016).

59 Imamura, H. *et al.* Visualization of ATP levels inside single living cells with fluorescence resonance energy transfer-based genetically encoded indicators. *Proc. Natl. Acad. Sci. USA* **106**, 15651-15656 (2009).

60 De Col, V. *et al.* ATP sensing in living plant cells reveals tissue gradients and stress dynamics of energy physiology. *eLife* **6**, e26770 (2017).

61 Cotilla-Sanchez, E., Hines, P. D. H. & Danforth, C. M. Predicting Critical Transitions From Time Series Synchrophasor Data. *IEEE Transactions on Smart Grid* **3**, 1832-1840 (2012).

62 Hsieh, C.-h., Glaser, S. M., Lucas, A. J. & Sugihara, G. Distinguishing random environmental fluctuations from ecological catastrophes for the North Pacific Ocean. *Nature* **435**, 336-340 (2005).

63 Chih-hao Hsieh, Christian Anderson & George Sugihara. Extending Nonlinear Analysis to Short Ecological Time Series. *The American Naturalist* **171**, 71-80 (2008).

64 Sugihara, G. *et al.* Distinguishing error from chaos in ecological time series. *Philos. Trans. R. Soc. Lond. B.* **330**, 235-251 (1990).

Supplementary Files

This is a list of supplementary files associated with this preprint. Click to download.

- DEVSI20020225.docx